Journal of Applied Fluid Mechanics, Vol. 15, No. 3, pp. 673-685, 2022.
Available online at www.jafmonline.net, ISSN 1735-3572, EISSN 1735-3645.
https://doi.org/10.47176/jafm.15.03.33327

Research on the Modified Mathematical Prediction Model of Impeller Cover Side Cavity Liquid Pressure for Centrifugal Pumps

J. L. Zeng[1†], Z. L. Liu [1,2], Q. Huang [1], H. Quan [1,2] and A. C. Shao [3]

[1] *School of Energy and Power Engineering, Lanzhou University of Technology, Lanzhou, Gansu Province, 730050, China*
[2] *Key Laboratory of Fluid Machinery and Systems, Lanzhou, Gansu Province, 730050, China*
[3] *Preeminence Pump Co., Ltd, Songxi, Fujian Province, 353500, China*

†*Corresponding Author Email: 15193110850@163.com*

(Received September 3, 2021; accepted January 15, 2022)

ABSTRACT

Accurate calculation of pressure distribution in the impeller cover side cavity is the key to predict the axial force of centrifugal pump. The existing calculation models almost does not involve the prediction of cavity pressure when the radial clearances of different sealing rings are matched with the diameter of different balance holes. On the basis of the original prediction model of pump cavity pressure, a mathematical model of pressure distribution of impeller cover side cavity with different radial clearance of sealing ring and the diameter of balance hole was established by introducing potential head correction coefficient and flow proportional coefficient. In order to improve the calculation accuracy of rotation coefficient for rear pump cavity, the balance aperture length ratio and the rotation undetermined coefficient were introduced in the calculation equation of original rotation coefficient. A test bed for pressure and leakage was designed and established, and the pressure of impeller cover side cavity and balance hole leakage was systematically tested when the radial clearance of sealing ring and the diameter of balance hole were different. Experimental results showed that the radial clearance of rear sealing ring and the diameter of balance hole had different effects on the radial pressure gradient of pump cavity. The diameter of balance hole had little effects on the pressure of the front pump cavity. When the clearance of the front and rear sealing rings were the same, the pressure of rear pump cavity was generally higher than that of the front pump cavity. For the equilibrium chamber liquid, increasing the diameter of balance hole could relieve the pressure, and increasing the radial clearance of sealing ring could increase the pressure. Combined with the test data, the potential head correction coefficient, the rotation undetermined coefficient and the flow proportional coefficient of different specific areas were calibrated, with a specific solution equation. In this study, the reliability of the proposed pressure mathematical model for impeller cover side cavity was verified by three cases. The results showed that the theoretical prediction value was more consistent with the actual measured value, proving that the proposed mathematical model had high accuracy and universality.

Keywords: Centrifugal pump; Pump cavity; Equilibrium chamber; Leakage; Axial force; Experimental study.

NOMENCLATURE

A_1	cross-sectional area of radial clearance of sealing ring	$\bar{p}$	pressure loss coefficient of equilibrium chamber
A_2	total area of balance holes	q_1	leakage of the sealing ring
$\bar{A}$	specific area	q_2	leakage of balance holes
b_1	radial clearance of the front sealing ring	Q	design flow rate of pump
b_2	radial clearance of the rear sealing ring	r	radius of the pressure measuring point
d	diameter of balance holes	r_1	radius of pump cavity outlet
D	diameter of impeller	r_2	radius of impeller
D_m	diameter of sealing ring	$\bar{r}$	relative radius, $\bar{r} = r/r_2$
H	pump operating head	R_{eu}	rotating Reynolds number at the outlet of

H_p	potential head at the blade outlet
H_t	theoretical head of pump
k	rotation coefficient
k_1	rotation coefficient of front pump cavity
k_2	rotation coefficient of rear pump cavity
L_1	length of sealing ring
L_2	length of balance holes
n	rotating speed
p	pressure at any radius of the pump cavity
p_1	pump inlet pressure
p_2	outlet pressure of impeller
p_3	inlet pressure of the pump cavity
p_4	inlet pressure of sealing ring clearance
p_5	outlet pressure of sealing ring clearance
p_6	pressure of equilibrium chamber
	impeller
u_2	circumferential velocity at the outlet of impeller, $u_2 = 2n\pi r_2/60$
z	number of balance holes
δ	rotation undetermined coefficient
φ_1	flow coefficient of the sealing ring
φ_2	flow coefficient of the balance holes
$\bar{\varphi}$	flow Proportional coefficient
σ	potential head correction coefficient
σ_1	potential head correction coefficient of front pump cavity
σ_2	potential head correction coefficient of rear pump cavity
η	pump efficiency
η_h	hydraulic efficiency
ρ	density of fluid
ν	coefficient of kinematic viscosity

1. INTRODUCTION

The axial force will be produced during the operation of centrifugal pump, and the unbalanced axial force will endanger the safety and stability during the operation. Therefore, it is necessary to accurately predict the size of axial force, and then select the appropriate axial force balancing device in the design for centrifugal pump Gülich (2008). The double sealing ring impeller with balance holes has simple structure and remarkable balance effect, so it is widely used in the design of centrifugal pump. For the centrifugal pump with this kind of impeller, the cavity formed by the impeller cover outside plate and the pump shell inside, is called the impeller cover side cavity, which mainly includes the front pump cavity, rear pump cavity and equilibrium chamber. The cover force on the impeller for the liquid in the impeller cover side cavity is the main component of axial force Guan (2011). Therefore, the accurate calculation of the pressure distribution in the impeller cover side cavity is the key to predict the axial force.

In the traditional method, the flow in the impeller cover side cavity is simplified as the flow in the dynamic and static cavity, and the ratio of the liquid rotation angular velocity in the core area to the impeller angular velocity is defined as the rotation coefficient, which is closely related to the pressure distribution and leakage in the cavity (Launder *et al.* 2010; Will *et al.* 2012; Huang *et al.* 2020). In Poncet (2005), the effects of Reynolds number and cavity aspect ratio on the rotation coefficient were studied, and the mathematical expression of rotation coefficient determined by leakage coefficient was given. On this basis, the liquid flow model of the pump cavity was also established in Yang *et al.* (2003), and the effects of Reynolds number and leakage on the rotation coefficient were studied as well. It pointed out that the rotation coefficient was about 0.48 with constant leakage, and the leakage had little effect on the rotation coefficient with constant Reynolds number. Li (2013) studied the influence of the radial clearance of sealing ring and the liquid viscosity on the liquid rotation coefficient of pump cavity, which showed that with the increase of the radial clearance of the sealing ring, the liquid rotation coefficient in the pump cavity increased. When the radial clearance of rear sealing ring was the same, the liquid rotation coefficient of rear pump cavity was slightly lower than that of the front pump cavity, and it was more obvious when the liquid viscosity was lower. The above literatures are all estimates of cavity leakage in the estimation of rotation coefficient, but the exact calculation of cavity leakage has not been solved.

In recent years, Computational Fluids Dynamics (CFD) method has become an important means for predicting the axial force. By applying this method, the detailed pressure distribution in pump cavity and equilibrium chamber can be obtained, and the coupling relationship between the pressure distribution and the axial force can be predicted (Dong *et al.* 2018; Dong *et al.* 2021). However, the accuracy for the calculation results of CFD method has been generally verified by the external characteristics of pump, and reliable pump performance information is usually not available at the initial stage of centrifugal pump design (Cao *et al.* 2015; Cheng *et al.* 2020; Han *et al.* 2012; Kim *et al.* 2020; Qian *et al.* 2021).

The one-dimensional theoretical model based on the experimental study can easily and rapidly predict the pressure distribution in the impeller cover side cavity with acceptable accuracy. Bruurs *et al.* (2017) proposed a hybrid algorithm for axial forces prediction, which took the results of CFD as boundary conditions for the theoretical calculation, thus reducing its cost. Zhang *et al.* (2019) established an integrated mathematical model for predicting the

liquid radial pressure distribution in pump cavity and the leakage of balance holes, and proposed that the theoretical value of the correction coefficient of the pressure loss term in pump cavity was 1.2. The inlet pressure correction coefficient of pump cavity and the flow coefficient of balance holes were calibrated by the experimental method. A test method for calibrating the pump cavity pressure prediction model was proposed in Elicio and Annese (2019). The pressure of the front and rear pump cavities for a single-stage model pump was measured, and the sensitivity analysis of the influence of inlet eddy current coefficient and rotation factor on the prediction model of pump chamber pressure was carried out. Gu *et al.* (2020) established a new one-dimensional pressure model to predict the pressure of pump cavity at different rotational speeds. Combined with the measured data of a centrifugal pump with variable rotational speeds, the high accuracy of the pressure model was verified. The pressure of pump cavity was proportional to the square of the rotational speed. The mathematical model of the equilibrium chamber pressure has been established in Liu *et al.* (2013), but the radial clearance of rear sealing ring and the flow coefficient of balance holes have been idealized, with some limitations in the engineering application. The radial clearance of sealing ring and the diameter of balance hole are the main geometric factors affecting the pressure distribution in the impeller cover side cavity. Due to the differences in working environment and mechanical design, different types of centrifugal pumps often adopt different sealing rings and balance holes in different sizes. Any changes of the above two factors will change the pressure distribution in impeller cover side cavity. Therefore, it is of great significance to predict the pressure in the cavity accurately when the radial clearances of different sealing rings are matched with different diameters of balance holes, but there are very few literatures on this aspect.

A mathematical model for the pressure distribution of impeller cover side cavity was established when the radial clearance of sealing ring and the diameter of balance holes changed. The pressure in impeller cover side cavity and the leakage of balance holes with different radial clearances of sealing ring and the diameter of balance holes were systematically tested. Combined with the test data, the rotation undetermined coefficients, potential head correction coefficients, and flow proportional coefficients of different specific areas were calibrated, and specific solution equations were given, which provided a new method for fast and accurate prediction of pressure distribution in impeller cover side cavity.

2. MATHEMATICAL MODEL OF PRESSURE DISTRIBUTION IN THE IMPELLER COVER SIDE CAVITY

Figure 1 shows the geometric model of the impeller cover side cavity, the left cavity of impeller cover is the front pump cavity, and the right cavity of impeller cover includes the rear pump cavity and the equilibrium chamber. During the operation of centrifugal pump, a part of the high pressure liquid at the outlet of impeller flows into the front and rear pump cavities, in the way that the liquid in front pump cavity flowed directly into the inlet of impeller through the radial clearance of front sealing ring, and the liquid in rear pump cavity flowed into the equilibrium chamber through the radial clearance of rear sealing ring. The liquid in equilibrium chamber then returned to the inlet of impeller through balance holes of impeller.

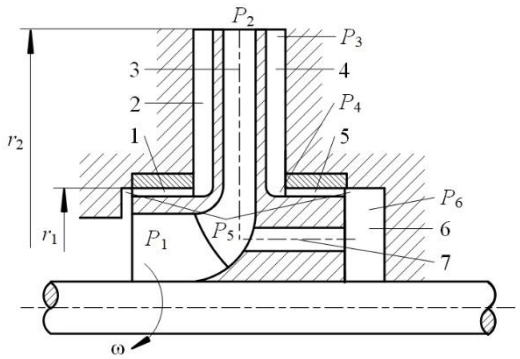

Note: 1. Radial clearance of front sealing ring; 2. Front pump cavity; 3. Impeller; 4. Rear pump cavity; 5. Radial clearance of rear sealing ring; 6. Equilibrium chamber; 7. Balance holes

Fig. 1. Geometric model of impeller cover side cavity.

2.1 Mathematical Model of Pressure Distribution in Pump Cavity

When the liquid in pump cavity rotates as a rigid body, the mathematical model of pressure distribution in pump cavity with radial direction is Gülich (2008):

$$p = p_3 - \frac{1}{2}\rho k^2 u_2^2 \left(1 - r^2 / r_2^2\right) \tag{1}$$

where ρ is the density of transport medium, k is the rotation coefficient, u_2 is the circumferential velocity at the outlet of impeller, ($u_2 = 2n\pi r_2 / 60$), r is the radial radius of any point in pump cavity.

In order to calculate the inlet pressure of pump cavity p_3, the potential head correction coefficient σ was introduced, which was defined as the ratio of pressure difference between the inlet and outlet of pump cavity and impeller potential head, essentially reflecting the pressure drop caused by the impeller unit potential head in pump cavity flow channel. that is,

$$\sigma = (p_3 - p_5)/(\rho g H_p) \tag{2}$$

where, H_p is the potential head at the blade outlet. The H_p represents the pressure energy obtained by the liquid passing through the impeller, which can be calculated with the following equation Guan (2011):

$$H_p = H_t \left(1 - \frac{g H_t}{2u_2^2}\right) \tag{3}$$

where H_t is the theoretical head of pump, $H_t = H/\eta_h$, H is the pump operating head, η_h is the hydraulic efficiency, $\eta_h = 1 + 0.0835\lg\sqrt[3]{Q/n}$, Q is the design flow rate of pump, n is rotation speed.

For the front pump cavity, if the pump inlet pressure p_1 is uniformly distributed with the radial direction, then $p_5 = p_1$. And the potential head correction coefficient of front pump cavity σ_1 can be expressed as follows:

$$\sigma_1 = (p_3 - p_1)/(\rho g H_p) \tag{4}$$

For the rear pump cavity, the numerical calculation of liquid flow in equilibrium chamber of centrifugal pump showed that the liquid flow in equilibrium chamber was a two-dimensional viscous laminar flow composed of circumferential shear flow and radial pressure differential flow, under the same flow conditions, the pressure in the equilibrium chamber increases uniformly with the increase of radius, but the increase was very small Dong *et al*. (2021). Since the radial and axial dimensions of equilibrium chamber were generally small, it could be considered that the pressure of equilibrium chamber was uniformly distributed with the radial direction, namely $p_5 = p_6$, then the potential head correction coefficient of rear pump cavity σ_2 can be expressed as:

$$\sigma_2 = (p_3 - p_6)/(\rho g H_p) \tag{5}$$

In order to distinguish easily, k_1 represents the rotation coefficient of front pump cavity and k_2 represents the rotation coefficient of rear pump cavity. Equation (4) can be substituted into Eq. (1), and the mathematical model of the pressure in front pump cavity can be obtained as below:

$$p = \sigma_1 \rho g H_p - \frac{1}{2}\rho k_1^2 u_2^2 \left(1 - \frac{r^2}{r_2^2}\right) + p_1 \tag{6}$$

Equation (5) can be substituted into Eq. (1), and the mathematical model of the pressure in rear pump cavity can be obtained as below:

$$p = \sigma_2 \rho g H_p - \frac{1}{2}\rho k_2^2 u_2^2 \left(1 - \frac{r^2}{r_2^2}\right) + p_6 \tag{7}$$

When the impeller rotates, the liquid in the pump cavity also rotates under the friction of the impeller cover. The angular momentum of the mainstream liquid at the impeller outlet can be brought into the pump cavity by the liquid leakage, thus enhancing the rotation of the liquid in the pump cavity and having an important impact on the pressure distribution in the pump cavity. Therefore, the accurate prediction of k is the technical guarantee to improve the calculation accuracy of the pump cavity pressure mathematical model. k is a function of the leakage of pump cavity, the greater the k, the greater the pressure drop in pump cavity, the smaller the pressure difference between the inlet and outlet of sealing ring and the resulting leakage, and k decreases as the leakage decreases Poncet (2005). Therefore, the k and the leakage of pump cavity are interdependent and restrict each other. Several methods for estimating k were given in the reference Gülich (2008), including geometric parameter method, equation method, graphic method and so on. Among them, the geometric parameter method is conducted according to the radial clearance and length of sealing ring, and the rotating Reynolds number at the outlet of impeller. In this paper, the k was estimated with the geometric parameter method. The details were as follows:

The calculation equation of the k_1 is Gülich (2008):

$$k_1 = 0.9\left(R_{eu}^{0.3}\frac{b_1 r_1}{2r_2^2}\sqrt{\frac{b_1}{L_1}}\right)^{0.087} \tag{8}$$

where R_{eu} is the rotating Reynolds number at the outlet of impeller, b_1 is the radial clearance of front sealing ring, L_1 is the length of sealing ring.

$$R_{eu} = r_2 u_2/\nu \tag{9}$$

where ν is the coefficient of kinematic viscosity.

Equation (8) covers the influence of the radial clearance and axial length of sealing ring on the rotation coefficient, which can predict the k_1 accurately. However, the liquid leakage in rear pump cavity was restricted by rear sealing ring and balance holes, while Eq. (8) did not include the influence of the balance hole geometry on the rotation coefficient. Therefore, estimating the k_2 with Eq. (8) is unreliable, which still needs to be improved. Combined with the actual situation, the length ratio of balanced holes was introduced into Eq. (8) to describe the influence of the geometric size of balanced holes on the rotation coefficient. As a result, the estimation equation of the k_2 can be obtained as follows:

$$k_2 = 0.9\left(R_{eu}^{0.3}\frac{b_2 r_1}{2r_2^2}\sqrt{\frac{b_2}{L_1} + \frac{d}{L_2}}\right)^{\delta} \tag{10}$$

where b_2 is the radial clearance of rear sealing ring, d is the diameter of balance holes, L_2 is the length of balance holes, δ is the rotation undetermined coefficient.

2.2 Mathematical Model of Equilibrium chamber Pressure

The pressure of equilibrium chamber can be affected by rear sealing ring and balance holes, and the effect of sealing ring and balance holes on the pressure of equilibrium chamber can be achieved by adjusting the leakage. According to the continuity formula of hydrodynamics, the leakage of rear sealing ring of centrifugal pump is equal to that of the balance holes.

The equation for calculating the leakage of sealing ring can be expressed as below Guan (2011):

$$q_1 = \varphi_1 A_1 \sqrt{2g\left(\frac{p_4}{\rho g} - \frac{p_6}{\rho g}\right)} \tag{11}$$

where q_1 is the leakage of sealing ring, φ_1 is the flow coefficient of sealing ring, A_1 is the cross-sectional area of radial clearance of sealing ring, $A_1 = D_m \pi b_2$, D_m is the diameter of sealing ring.

The liquid flow in balance holes can be simplified to the outflow of submerged nozzle, and the leakage of balance holes can be obtained from the following formula Liu *et al*. (2017):

$$q_2 = \varphi_2 A_2 \sqrt{2g\left(\frac{p_6}{\rho g} - \frac{p_1}{\rho g}\right)} \tag{12}$$

where q_2 is the leakage of balance holes, φ_2 is the flow coefficient of balance holes, A_2 is the total area of balance holes, $A_2 = \pi d^2 z/4$, z is the number of balance holes.

It can be obtained from this equation that $q_1 = q_2$:

$$\left(\frac{\varphi_2 A_2}{\varphi_1 A_1}\right)^2 = \frac{p_4 - p_6}{p_6 - p_1} \tag{13}$$

If the numerator on the right side of the equation is simultaneously added or subtracted by p_1, and the numerator denominator is divided by $\rho g H_p$ equation at the same time, then Eq. (13) can be expressed as follows:

$$\left(\frac{\varphi_2 A_2}{\varphi_1 A_1}\right)^2 = \left(\frac{p_4 - p_1}{\rho g H_p} - \frac{p_6 - p_1}{\rho g H_p}\right) \Big/ \left(\frac{p_6 - p_1}{\rho g H_p}\right) \tag{14}$$

According to Eq. (7), p_4 can be expressed as:

$$p_4 = \sigma_2 \rho g H_p - \frac{1}{2}\rho k_2^2 u_2^2 \left(1 - \frac{r_1^2}{r_2^2}\right) + p_6 \tag{15}$$

In order to facilitate the calculation of equilibrium chamber pressure between similar pumps, the following dimensionless characteristic parameters were introduced, including specific area $\bar{A}$ and the pressure loss coefficient of equilibrium chamber $\bar{p}$, which are defined as follows Liu *et al*. (2007):

The $\bar{A}$ is defined as:

$$\bar{A} = A_2 / A_1 \tag{16}$$

The specific area essentially reflects the degree of diffusion and contraction of the inlet and outlet of equilibrium chamber.

The $\bar{p}$ is defined as:

$$\bar{p} = \left(p_6 - p_1\right) \Big/ \left(\rho g H_p\right) \tag{17}$$

The $\bar{p}$ essentially reflects the pressure loss of impeller unit potential head at balance holes.

The φ_2 depends on the shrinkage of cross section of balance holes and the local resistance loss at the outlet Zhang (2013). During the operation of pump, the flow pattern is very complex due to the mixing between the liquid at the outlet of balance holes with the mainstream convection at the inlet of impeller, making the shrinkage of cross section and local resistance loss difficult to determine. The φ_1 depends on the resistance coefficient and the fillet coefficient of sealing ring Guan (2011), because the resistance coefficient of the inlet and outlet of sealing ring is very sensitive to the change of the radial clearance and inlet shape of the sealing ring, the calculation of the flow coefficient of the balance hole and the sealing ring using the traditional calculation formula will produce a large error. Therefore, a flow proportional coefficient $\bar{\varphi}$ is introduced, which is defined as:

$$\bar{\varphi} = \varphi_2 / \varphi_1 \tag{18}$$

The mathematical model of the $\bar{p}$ can be obtained by substituting the Eqs. (15), (16), (17), (18) into Eq. (14).

$$\bar{p} = \frac{\sigma_2 - \dfrac{k_2^2 u_2^2 \left(1 - \dfrac{r_1^2}{r_2^2}\right)}{2gH_p}}{\bar{\varphi}^2 \bar{A}^2} \tag{19}$$

So far, a complete mathematical model of pressure distribution in impeller cover side cavity has been constructed. According to Eq. (8), the rotation coefficient of front pump cavity k_1 can be calculated, and the substitution Eq. (6) can calculate the pressure of front pump cavity; According to Eq. (10), the rotation coefficient of rear pump cavity k_2 can be calculated, and the substitution Eq. (19) can calculate the pressure loss coefficient $\bar{p}$ of equilibrium chamber at a given specific area, and then replace $\bar{p}$ into Eq. (17) to deduce the pressure of equilibrium chamber p_6; the calculated p_6 and k_2 plug-in Eq. (7) can be used to calculate the pressure of rear pump cavity. It should be noted that the pump inlet pressure p_1 needs to be actually measured, and the σ, δ, and $\bar{\varphi}$ is the functions for the specific area $\bar{A}$, which needs to be determined by test.

3. TEST METHODS

3.1 Test Devices

In this study, IS80-50-315 centrifugal pump was taken as the test pump. Its performance parameters and main geometric parameters are shown in Table 1.

A test-bed for the pressure of impeller cover side cavity and the leakage of balance holes for the centrifugal pump was designed and established, as

Table 1 Performance parameters and main geometric parameters of IS80-50-315 centrifugal pump

Description	Parameter	value
Design flow rate of pump	Q (m^3/h)	25
Pump operating head	H (m)	32
Rotating speed	n (rpm)	1450
Pump efficiency	η (%)	52
diameter of impeller	D (mm)	315
Diameter of sealing ring	D_m (mm)	90
Radial clearance of the front sealing ring	b_1 (mm)	0.2
Radial clearance of the rear sealing ring	b_2 (mm)	0.2
Length of sealing ring	L_1 (mm)	15
Diameter of balance holes	d (mm)	6
Length of balance holes	L_2 (mm)	28
Number of balance holes	z	5

Note: 1. Motor; 2. Rotational speed torque meter; 3. Test pump; 4. Storage bucket; 5. Pump outlet pipeline; 6. Gate valve; 7. 1# Electromagnetic; 8. Water tank; 9. Pressure sensor; 10. Pressure stabilizing device; 11. Regulating valve; 12. Pump inlet pipeline; 13. 2# Electromagnetic flowmeter; 14. Drainage tube

Fig. 2. Test-bed

shown in Fig. 2. During the test, the liquid flow into the test pump from the water tank through the inlet pipeline of pump, and then flow back to the water tank through the outlet pipeline of pump.

A speed torque sensor was installed between the motor and the test pump to measure the speed, torque and input power of the test pump, with the measurement accuracy of rotational speed, torque and input power of 0.1%, 0.3% and 0.5%, respectively. In addition, the flow was measured by an electromagnetic flowmeter with an accuracy of 0.5%.

3.2 Pressure Measurement of Impeller Cover Side Cavity

The pressure measurement of impeller cover side cavity belongs to multi-point measurement, and the pressure fluctuation of pump cavity will affect the measurement accuracy. In this paper, the pressure points of front and rear pump cavities for the measurement were arranged on the characteristic section of volute, namely, on the axial plane of the eighth section. The pressure testing device of impeller cover side cavity is shown in Fig. 3. The radius of pressure measuring hole center in the front pump cavity were 49mm, 76mm, 94mm, 116mm, 134mm, 149mm, 155mm, respectively. The radius of pressure measuring hole center in the rear pump cavity were 49mm, 76mm, 94mm, 105mm, 116mm, 134mm, 149mm, 155mm, respectively, and the radius of pressure measuring hole center in the equilibrium chamber was 45mm.

In order to ensure the stability of the measurement, the pressure stabilizing device was specially designed, as shown in Fig. 4., which was equipped with a precision pressure gauge with an accuracy of 0.4 and a capacitive pressure sensor with an accuracy of 0.5. All the pressure measuring holes were connected with the pressure stabilizing device through the pressure hose, and any pressure measuring hole can be connected to the pressure stabilizing device by switching the throttle valve. The indicated values of pressure gauge and the capacitive pressure sensor can be mutually confirmed and the measured pressure can be tested as well. The total uncertainty of pressure measurement was 0.63%.

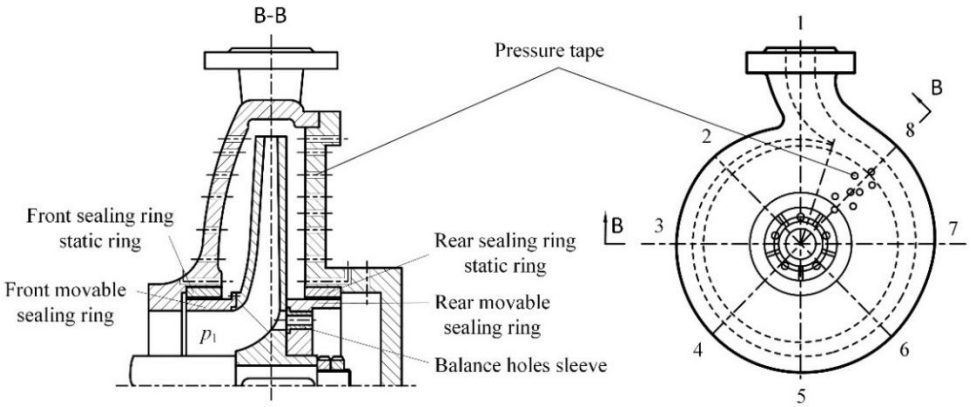

Fig. 3. Pressure testing device for impeller cover side cavity.

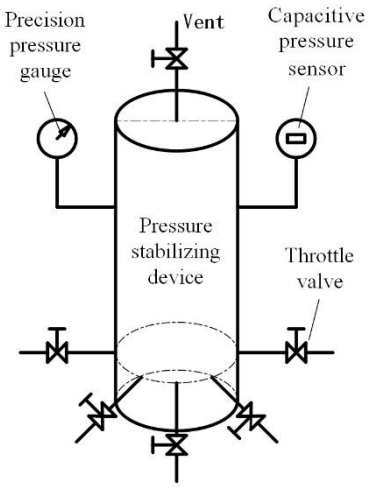

Fig. 4. Pressure stabilizing device.

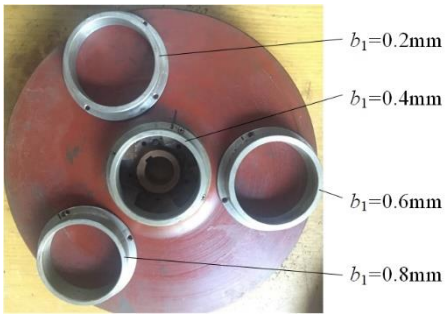

(a) Front movable sealing ring

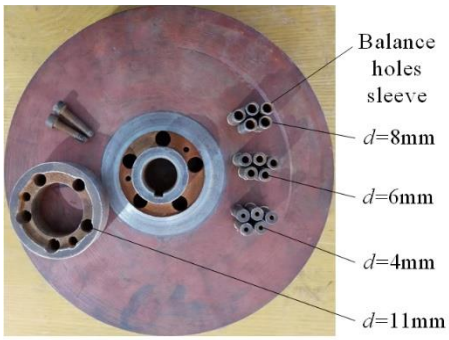

(b) Rear movable sealing ring

Fig. 5. Movable sealing ring and impeller.

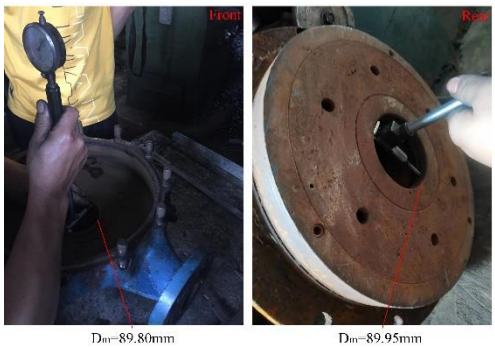

Fig. 6. Inner diameter test drawing for static ring of sealing ring.

In order to realize the different matching relationship between the radial clearance of front and rear sealing rings and the diameter of balance holes on the same impeller, the front movable sealing ring, rear movable sealing ring and balance hole sleeve were specially designed and assembled on the impeller to form the impeller assembly diagram, as shown in Fig. 5. The rear movable sealing ring was provided with balance holes, with the inner diameter of 11mm. In addition, the balance hole sleeve can be installed on the rear movable sealing ring, with the inner diameter of 4mm, 6mm, and 8mm, respectively, and the outer diameter of 11mm.

The accurate radial clearance value of sealing can ensure the test accuracy. Therefore, the inner diameter of static ring of front and rear sealing rings was specially measured before the test. The inner diameter of static ring of the front and rear sealing rings was 89.80mm and 89.95mm respectively. According to the measurement results, the radial clearance of front sealing ring b_1 were 0.2mm, 0.4mm, 0.6mm, and 0.8mm, and those of rear sealing ring b_2 were 0.2mm, 0.4mm, 0.6mm, 0.8mm, and 1mm, respectively. Figure 6 is the inner diameter test drawing for static ring of sealing ring. The balance holes sleeve was replaced under the radial clearance of each sealing ring to realize the measurement of the pressure on impeller cover side cavity with different specific surface areas.

3.3 Measurement of Leakage

In order to measure the leakage of balance holes, the motor was set on the inlet side of impeller, a regulating valve was installed on the rear pump cover, and a section of water diversion pipe connected the regulating valve to the electromagnetic flowmeter, which was connected to the pump inlet pipeline by a three-way pipe to form a closed loop. When measuring, the regulating valve was closed for the first time, and after the pump ran stably, the pressure of the radial clearance inlet of rear sealing ring (the pressure hole with the radius of 49mm) and the radial clearance outlet of rear sealing ring (the pressure hole with the radius of 45mm) were measured. Then, balance holes of impeller were plugged, to let the pump work under the same working conditions, then the control valve was opened, so that the pressure at the inlet and outlet of rear sealing ring's radial clearance was equal to that when balance holes was opened. At this point, the indicator value of the 2# electromagnetic flowmeter is the leakage amount of the balance hole at the corresponding to the radial clearance of the rear sealing ring and the diameter of the balance hole. In order to verify the reliability of the above method in measuring the leakage of balance holes, the liquid at the outlet of control valve was led to the storage bucket as shown in Fig. 7.

Fig. 7. Field diagram of leakage calibration of balance holes.

The volume V of bucket was known, and the time t of bucket filled with water was recorded. The leakage of balance holes was obtained by dividing V by t. Comparing the measurement results of the two methods, it can be found that the relative error was less than 2.64%, indicating that the leakage measurement method proposed in this paper was reliable. The total uncertainty of leakage measurement was 0.71%.

4. RESULTS AND ANALYSIS

4.1 Pressure Measurement Results of Impeller Cover Side Cavity

In order to study the pressure distribution of impeller cover side cavity with different specific areas, two pressure measurement schemes were designed. Scheme 1: Under the condition of $b_1 = 0.4$ mm, the pressure of rear pump cavity and equilibrium chamber were tested when b_2 were 0.2mm, 0.4mm, 0.6 mm, 0.8mm, 1mm, respectively, and d were 4mm, 6 mm, 8mm, and 11mm, respectively. Scheme 2: Under the condition of $b_2 = 0.2$ mm, the pressure of front pump cavity was measured when b_1 were 0.2mm, 0.4mm, 0.6 mm, and 0.8mm, respectively, and d were 4mm, 6 mm, 8mm, and 11mm, respectively. When the design flow rate of test pump was $Q = 25\,\mathrm{m^3/h}$, the measured rotation speed was

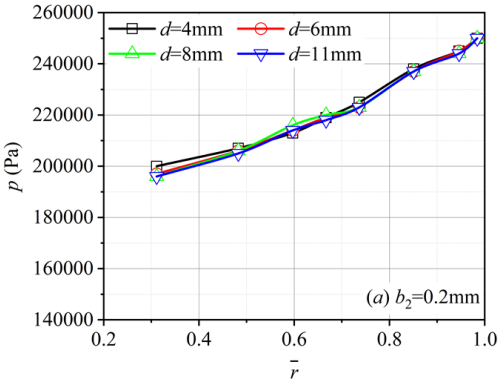

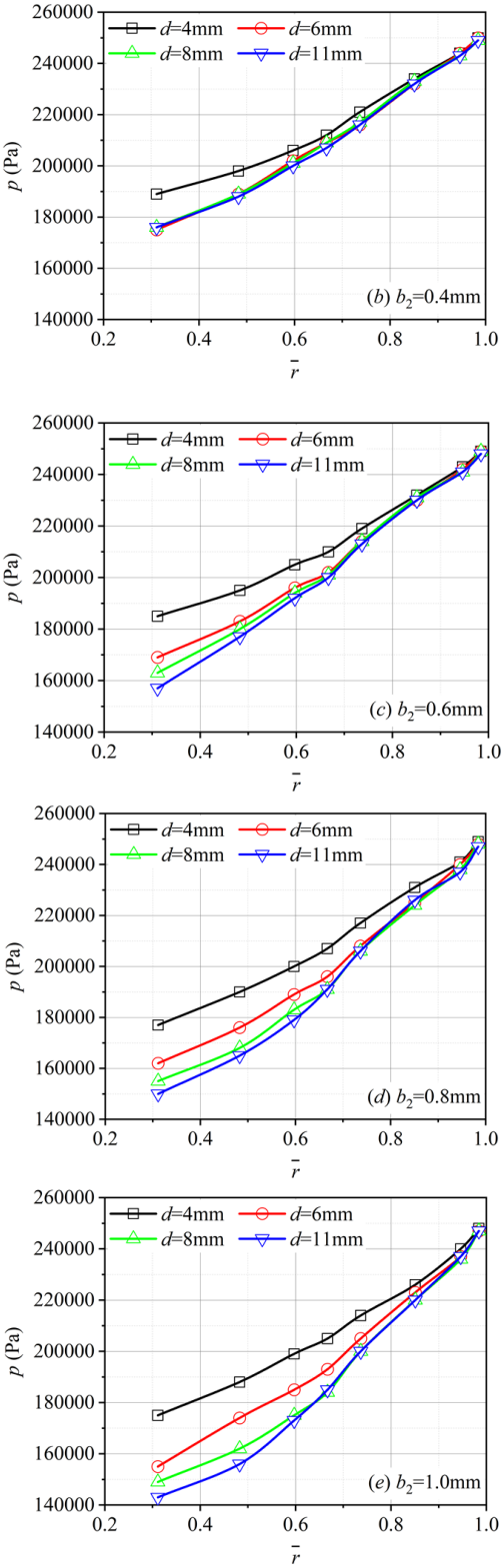

Fig. 8. Relation curve between pressure and relative radius of rear pump cavity.

$n = 1470$ rpm, the head was $H = 31.5$ m, and the impeller outlet potential head $H_p = 25.77$ m was calculated from Eq. (3). In Fig. 8, (a), (b), (c) and (d) are the test curves for the relationship between the pressure of rear pump cavity and the relative radius.

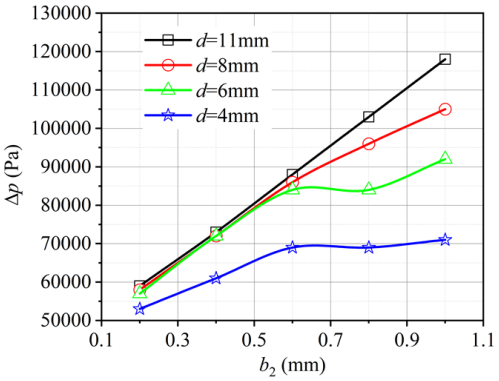

Fig. 9. Radial pressure difference of rear pump cavity.

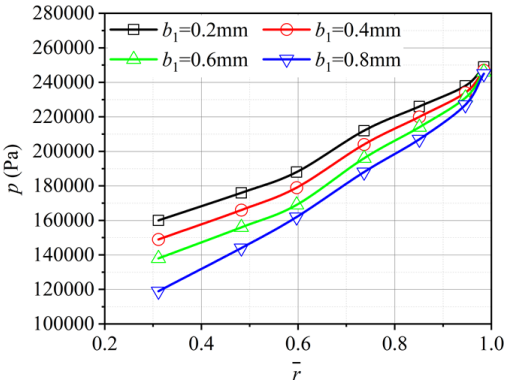

Fig. 10. Relation curve between pressure and relative radius of front pump cavity.

Among them, the relative radius is defined as the ratio of measuring point radius to impeller radius, with the equation of definition as $\bar{r} = r/r_2$. It can be seen from Fig. 8 that the pressure of rear pump cavity was distributed according to the parabola along the radius direction, and the greater the radius, the greater the pressure. When b_2 and d changed, the inlet pressure p_3 of pump cavity was basically unchanged. The radial pressure gradient of pump cavity increased as b_2 and d increased. Therefore, b_2 and d had different effects on the radial pressure gradient. Due to the same radius of pump cavity, the pressure difference between the inlet and outlet of rear pump cavity can reflect their radial pressure gradient.

In order to reflect the influence of b_2 and d on the radial pressure gradient of rear pump cavity directly, the changing curve of pressure difference between the inlet and outlet of rear pump cavity Δp with b_2 when d were 4mm, 6mm, 8mm, and 11mm respectively, which was drawn in Fig. 9.

It can be seen from Fig. 9 that when b_2=0.6 mm and $d = 6$ mm were taken as the boundary, $b_2 < 0.6$ mm, with the increase of b_2 , the peak of Δp increased linearly as b_2 increased. When b_2 was the same, the peak of Δp was the lowest when d was 4 mm, and when d were 6 mm, 8 mm and 11mm, the peak of Δp was almost the same. When $b_2 \geq 0.6$ mm, the variation trend of Δp with b_2 was greatly affected by d , and the smaller the d , the smaller the growth of Δp . According to the above analysis, b_2 played an important role in regulating the pressure of rear pump cavity when $b_2 < 0.6$ mm, and d played a major role in regulating the pressure of rear pump cavity when $b_2 \geq 0.6$ mm.

When the impeller rotated, the liquid in pump cavity also rotated with the friction of impeller cover. The liquid rotation will produce centrifugal force outward along the radius. The greater the rotation coefficient k and the radius of pump cavity, the greater the centrifugal force. At the same time, the liquid in pump cavity also flowed radially inward with differential pressure force at the inlet and outlet of pump cavity. The increase of b_2 or d will increase the leakage, so that the angular momentum of the mainstream liquid at the impeller outlet is brought into the pump cavity by the leakage liquid, thus enhancing the rotation of the liquid in pump cavity. Therefore, the greater the leakage, the larger the k , the stronger the centrifugal force of pump cavity liquid, leading to the increased pressure drop in pump cavity, the pressure difference between the inlet and outlet of sealing ring and the resulting leakage was smaller, and the k decreased with the decrease of leakage Poncet (2005). Therefore, the rotation coefficient and the pump cavity leakage were mutually dependent and constrained, which was the reason for the experimental phenomenon observed in Fig. 8 and Fig. 9.

The test also found that the change of d had almost no effect on the pressure of front pump cavity. Figure 10 only showed the pressure measurement results of front pump cavity when $d = 6$ mm.

According to the comparison between Fig. 8 and Fig. 10., the radial pressure gradient of front pump cavity was obviously larger than that of rear pump cavity with the same radial clearance of sealing rings. However, the pressure of rear pump cavity is usually higher than that in the front pump cavity, because the leakage of rear pump cavity was also restricted by balance holes with the same radial clearance of sealing ring, making the leakage of front pump cavity larger than that of rear pump cavity.

Figure 11 showed the experimental curve of equilibrium cavity pressure and pump inlet pressure changing with specific area.

Shown by Fig. 11., p_1 fluctuates within a very small range as $\bar{A}$ increases, and p_1 can be considered to remain unchanged. The relation curve between p_6 and $\bar{A}$ is approximately one part of the image of inverse proportional function. Combining with the definition of $\bar{A}$, it can be seen that p_6 is adjusted by b_2 and d together. When b_2 is small, d is large,

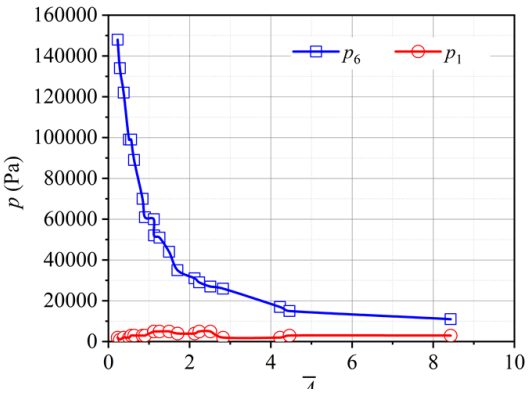

Fig. 11. Equilibrium chamber and pump inlet pressure.

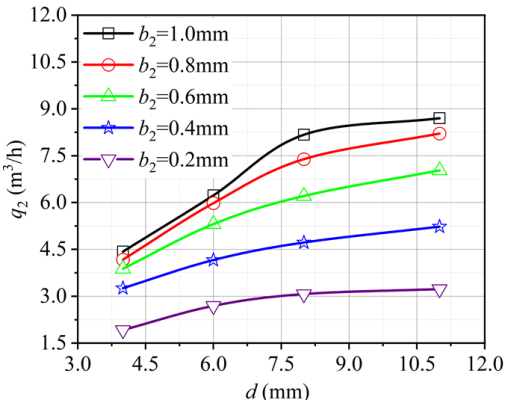

Fig. 12. Test results of leakage of balance holes.

P_6 is small. On the contrary, when b_2 is large, d is small, p_6 is large, Thus, increasing d can relieve the pressure of the liquid in equilibrium chamber, while increasing b_2 has the opposite effect against increasing d. The above phenomenon is caused by the change of linear loss when b_2 and d change, and the linear loss h_f can be expressed as:

$$h_f = \lambda \frac{l}{d_1} \frac{v^2}{2g} \tag{20}$$

where, λ is for the resistance coefficient, l is for linear length, d_1 is for the diameter, and v is for the mean velocity in section.

It can be seen from Eq. (20), when d remains unchanged as b_2 increases, the linear loss in the clearance of the rear sealing ring decreases, which increases the outlet pressure of the clearance of rear sealing ring, resulting in the increase of p_6. Similarly, when b_2 remains unchanged and d increases, the linear loss of balance hole decreases, while p_1 remains almost unchanged, which lowers the inlet pressure of balance hole and leads to A decrease in p_6.

The leakage of balance holes was measured when d were 4mm, 6mm, 8mm, and 11mm matching with b_2 of 0.2mm, 0.4mm, 0.6mm, 0.8mm, and 1.0mm, and the test results were drawn in Fig. 12.

From Fig. 12, with the increase of b_2 and d, the leakage amount of the equilibrium hole increases non-linearly, and the change rate gradually decreases. According to Eq. (20), when b_2 increases, h_f in the gap of rear sealing ring decreases, which is bound to cause the increase of q_1, but the increase of q_1 also leads to the increase of v in the gap of sealing ring, which makes h_f larger. Therefore, this is a process of promotion and reverse restriction. When b_2 further increases, the roles of such promotion and reverse restriction gradually tend to balance, which is the reason for the above experimental phenomenon. Similarly, when d increases, the change process of h_f in the balance hole is the same as that in the gap of the back seal ring when b_2 increases.

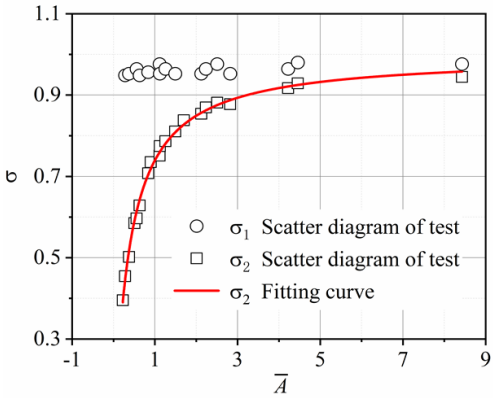

Fig. 13. Relationship between potential head correction coefficient and specific areas.

4.2 Determination of Potential Head Correction Coefficient

In order to determine the potential head correction coefficient of front and rear pump cavities with different specific surface areas $\overline{A}$, according to the Eq. (4) and Eq. (5) and the test data, σ_1 and σ_2 in the pressure measurement scheme were calculated. Then, the scatter diagram of variation with $\overline{A}$ was drawn as Fig. 13. From Fig. 13, σ_1 fluctuated slightly and σ_2 changed obviously as the $\overline{A}$ increased. In order to facilitate engineering application, the average value of σ_1 was 0.958 for different $\overline{A}$, and the mathematical expression describing the relationship between σ_2 and $\overline{A}$ was obtained through the regression analysis.

σ_2 mathematical expression is as follows:

$$\sigma_2 = 0.997\overline{A} \Big/ \left(0.35 + \overline{A}\right) \tag{21}$$

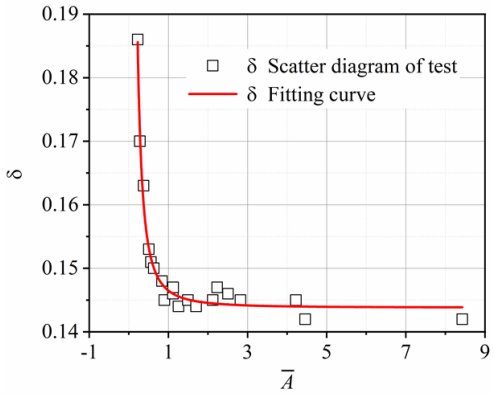

Fig. 14. Relation curve between rotation undetermined coefficient and specific areas.

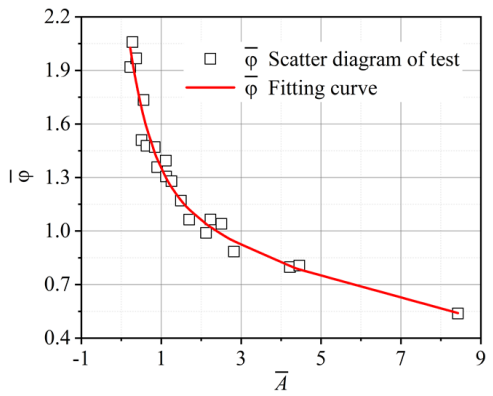

Fig. 15. Relationship between flow proportional coefficient and specific areas.

4.3 Determination of Rotation Undetermined Coefficient

In order to determine the δ for different $\bar{A}$, the test data in Fig. 8 were substituted Eq. (1), the rotation coefficient k_2 of each measuring point of rear pump cavity with different $\bar{A}$ was derived and averaged, and then the calculation results were substituted for the Eq. (10). The rotation coefficient δ of different $\bar{A}$ was deduced inversely, and the scatter diagram of δ and $\bar{A}$ was drawn in Fig. 14.

Referring to the regression analysis of the scatter diagram in Fig. 14, the mathematical expression characterizing the relationship between the δ and the $\bar{A}$ is obtained as below.

$$\delta=0.144+\frac{2.144}{1+\left(\frac{\bar{A}}{0.027}\right)^{1.85}} \tag{22}$$

4.4 Determination of Flow Proportion Coefficient

By substituting the measured values of p_1 and p_6 at given $\bar{A}$ and the measured value of discharge from balance holes in Eq. (12), φ_2 cycles of the corresponding $\bar{A}$ were calculated. Because q_1 and q_2 were equal when $\bar{A}$ was the same, φ_1 of the corresponding $\bar{A}$ was calculated by measuring the inlet and outlet pressure of rear sealing ring and replacing q_1 in Eq. (11). Then, the calculated φ_1 and φ_2 were substituted into Eq. (18), and the $\bar{\varphi}$ at given $\bar{A}$ was calculated. The scatter plot $\bar{\varphi}$ with $\bar{A}$ was drawn in Fig. 15, and the regression analysis was carried out, obtaining the mathematical expression characterizing the relationship between $\bar{\varphi}$ and $\bar{A}$.

$$\bar{\varphi}=1.13\exp\left(\frac{-\bar{A}}{0.58}\right)+1.06\exp\left(\frac{-\bar{A}}{6.8}\right)+0.23 \tag{23}$$

5. EXAMPLE VERIFICATION

The accuracy and universality of the pressure calculation model for impeller cover side cavity proposed in this paper were verified with the following three examples.

Example 1: In Tang (1987), the pressure at the radius of rear pump cavity of 110mm, 130mm, and 155 mm, and the pressure of equilibrium chamber when an IS200-150-315 centrifugal pump was working under the designed conditions were tested. The performance parameters of the test pump were as follows: $Q=200$ m^3/h, H=32 m, $n=1450$ rpm. The outer diameter of impeller was D=325 mm, and the diameter of sealing ring was $D_m=165$ mm. It is pointed out that the $\bar{A}=1$, and the $L_2=10$ mm, $L_1=18$ mm, as well as the radial clearance of sealing ring was $b_2=0.4$ mm. In the designed conditions, the $p_1=-25000$ Pa, $p_6=36800$ Pa. Calculating from Eq. (3), the outlet potential lift of impeller under the designed conditions was 25.75m, Eq. (17) and (19) show that the relative error between the predicted value of equilibrium chamber pressure and the measured value was only -3.9%. The pressure of equilibrium chamber predicted by Eq. (17) and Eq. (19) was $p_6=35370$ Pa. The pressure prediction and test results of rear pump cavity of the test pump were given in Fig. 16.

From the pressure curve of pump cavity in Fig. 16, the relative errors between the pressure test and theoretical calculation of rear pump cavity were -3.84% (110mm), -0.79% (130mm) and 2.2% (150mm), respectively, indicating that the calculation model proposed in this paper had high accuracy and universality.

Example 2: The equilibrium chamber pressure mathematical model proposed in this paper was adopted to calculate the pressure of equilibrium chamber of the test pump (IS80-50-315 centrifugal pump) under the designed conditions, when d were 6 mm and 8mm, respectively, b_2 were 0.2mm,

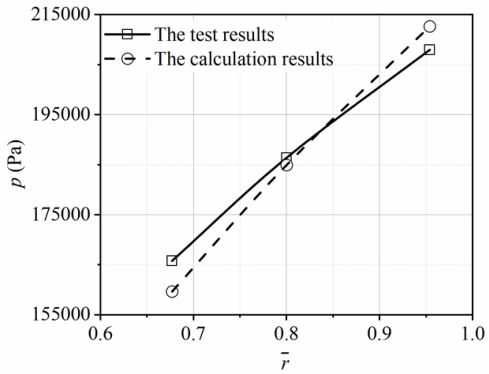

Fig. 16. Rear pump cavity pressure contrast diagram of the IS200-150-315 centrifugal pump.

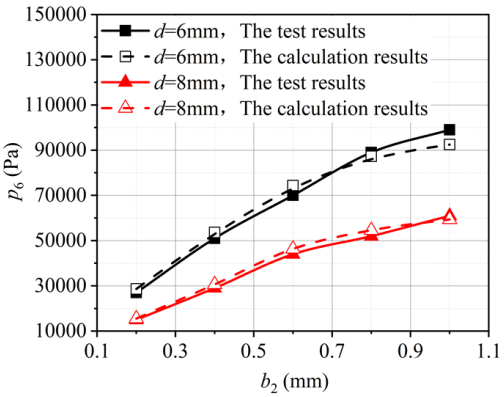

Fig. 17. Equilibrium chamber pressure contrast diagram of the IS80-50-315 centrifugal pump.

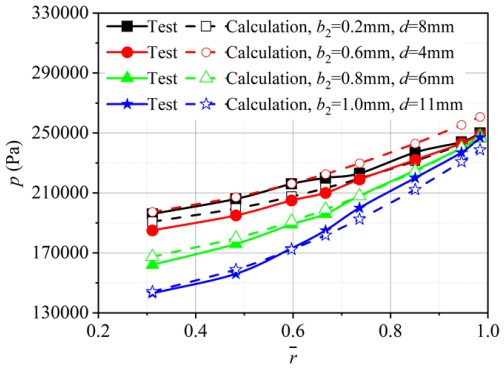

Fig. 18. Rear pump cavity pressure contrast diagram of the IS80-50-315 centrifugal pump.

0.4mm, 0.6 mm, 0.8mm, and 1mm, respectively. The comparison curve between theoretical calculation and measured results was drawn in Fig. 17.

In Fig. 17, the corresponding errors of the test and prediction curves were -6.15% ($b_2 = 0.2$ mm), -5.16% ($b_2 = 0.4$ mm), -6.25% ($b_2 = 0.6$ mm), 1.92% ($b_2 = 0.8$ mm), and 6.54% ($b_2 = 1.0$ mm) when d was 6mm, and -3.75% ($b_2 = 0.2$ mm), -5.64% ($b_2 = 0.4$ mm), -5.4% ($b_2 = 0.6$ mm), -5.02% ($b_2 = 0.8$ mm), and 2.63% ($b_2 = 1.0$ mm) when d was 8mm.

Example 3: According to the pressure calculation model of impeller cover side cavity proposed in this paper, the pressure of rear pump cavity under four conditions: $b_2 = 0.2$ mm matching $d = 8$ mm, $b_2 = 0.6$ mm matching $d = 4$ mm, $b_2 = 0.8$ mm matching $d = 6$ mm, $b_2 = 1.0$ mm matching $d = 11$ mm, was calculated respectively, and the theoretical calculation results and measured results were plotted in Fig. 18.

According to the results shown in Fig. 18, the deviation between the theoretical value and the experimental value in the other three matching relationships is very small, except that the calculated result of the condition $b_2 = 0.6$ mm matching $d = 4$ mm deviates slightly from the test result in the case. The minimum relative error between the theoretical value and the experimental value is -0.03% ($b_2 = 0.8$ mm, $d = 6$ mm, $\bar{r} = 0.95$), and the maximum relative error is 6.65% ($b_2 = 0.6$ mm, $d = 4$ mm, $\bar{r} = 0.31$). In addition, the variation trend of theoretical and experimental values with relative radius is consistent under the four matching relationships.

Combined with the above three examples, it can be seen that the calculation model proposed in this paper can predict the liquid pressure distribution in pump cavity and the liquid pressure in equilibrium chamber according to the needs of engineering applications.

6. CONCLUSIONS

Considering the influence of balance hole geometry size on the liquid flow state in rear pump cavity, the balance pore length ratio and the undetermined rotation coefficient were introduced into the original calculation formula of rotation coefficient, and the estimation method of liquid rotation coefficient in pump cavity of double-seal impeller pump with the balance hole was improved.

Experimental research indicated that in the adjustment for the pressure of rear pump cavity, the radial clearance of rear sealing ring was vital when $b_2 < 0.6$ mm, and the diameter of balance holes was vital when $b_2 \geq 0.6$ mm, thus, the diameter of balance hole played a major role in regulating the pressure of rear pump cavity. The change of balance hole diameter had little effect on the front pump chamber pressure. The pressure of rear pump cavity was generally higher than that of front pump cavity when the clearance of front and rear sealing rings was the same. For the liquid in equilibrium chamber, increasing the diameter of balance holes relieved the pressure, and increase the radial clearance pressurization of the rear seal ring.

Combined with the experimental data, the potential head correction coefficient, rotation undetermined coefficient and flow proportional coefficient under different specific area were calibrated, and the specific solution formula was given. The reliability of the mathematical model of the pressure in impeller cover side cavity was verified by three test examples.

The results showed that the mathematical model has high accuracy and universality.

ACKNOWLEDGEMENTS

This project was supported by the National Nature Science Foundation of China (Grant no. 51969014), and the Natural Science Foundation of Gansu Province (Grant no. 20JR5RA456), and the Outstanding Youth Foundation of Gansu Province (Grant no. 20JR10RA204).

REFERENCES

Bruurs, K. A. J., B. P. M. Van Esch and M. S. Vander Schoot (2017). Axial Thrust Prediction for a Multi-Stage Centrifugal Pump. *Proceedings of the ASME 2017 Fluids Engineering Division Summer Meeting*, Hawaii, USA 1-10.

Cao, W. D., X. Dai and Q. Hu (2015). Effect of impeller reflux balance holes on pressure and axial force of centrifugal pump. *Journal of Central South University* 22(5), 1695-1706.

Cheng, X. R., Z, Chang and Y. Jiang (2020). Study on the influence of the specific area of balance hole on cavitation performance of high- speed centrifugal pump. *Journal of Mechanical Science and Technology* 34(8), 3325-3334.

Dong, W. and W. L. Chu (2018). Numerical Investigation of Fluid Flow Mechanism in the Back Shroud Cavity of a Centrifugal Pump. *Journal of Applied Fluid Mechanics* 11(3), 709-719.

Dong, W., D. Chen and J. Sun (2021). Influence of Balance Hole Diameter on Leakage Flow of the Balance Chamber in a Centrifugal Pump. *Shock and Vibration*, 1-11.

Elicio, G. and F. Annese (2019). Experimental Approach to Predict the Residual Axial Thrust in Centrifugal Pumps. *Proceedings of the ASME-JSME-KSME*, San Francisco, USA.

Gu, Y. D., J. Pei and S. Yuan (2020). A Pressure Model for Open Roto-Stator Cavities: An Application to an Adjustable-Speed Centrifugal Pump with Experimental Validation. *Journal of Fluids Engineering* 142(10), 101301.

Guan, X. F. (2011). *Theory and design of modern pump*. China Astronautic Publishing House.

Gülich, J. F. (2008). *Centrifugal pumps*. 2nd ed, Springer-verlag, Berlin.

Han, W., W. Maa and R. N. Li (2012). The Numerical Analysis of Radial Thrust and Axial Thrust in the Screw Centrifugal Pump. *Procedia Engineering* 31, 176-181.

Huang, Q., Z. L. Liu and X. B. Wang (2020). Coupling Mechanism of Rotating Casing Effect and Impeller Structure of Roto-Jet Pump. *Shock and Vibration*, 1-13.

Kim, W. and J. Yun (2020). CFD Analysis on the Balancing Hole Design for Magnetic Drive Centrifugal Pumps. *Energies* 13(22).

Launder, B., S. Poncet and E. Serre (2010). Laminar, Transitional, and Turbulent Flows in Rotor-Stator Cavities. *Annual Review of Fluid Mechanics* 42(1), 229-248.

Li, W. G. (2013). Model of Flow in the Side Chambers of an Industrial Centrifugal Pump for Delivering Viscous Oil. *Journal of Fluids Engineering* 135(5), 51201.

Liu, Z. L., B. M. Wang and S. Liang (2007). Experimental study on the pressure in the equilibrium chamber of floating impeller. *Drainage and Irrigation Machinery* (04), 6-8.

Liu, Z. L., W. Dong and N. Zhang (2013). Calculation and validation of fluid pressure of equilibrium chamber in centrifugal pump. *Transactions of the Chinese Society of Agricultural Engineering* 29(20), 54-59.

Liu, Z. L., X. C. Chen and D. W. Wang (2017). Experiment and analysis of balance hole liquid leakage in centrifugal pump. *Transactions of the Chinese Society of Agricultural Engineering* 33(7), 67-74.

Poncet, S., M. P. Chauve and L.E. Gal P (2005). Turbulent rotating disk flow with inward throughflow. *Journal of Fluid Mechanics* 522, 253-262.

Qian, C., X. Luo and C. X. Yang (2021). Multistage pump axial force control and hydraulic performance optimization based on response surface methodology. *Journal of the Brazilian Society of Mechanical Sciences and Engineering* 43(3).

Tang, X. (1987). Exploration of pressure distribution law on back cover plate of centrifugal pump. *Hydraulic vane pump* (02), 30-34

Will, B., F. Benra and H. Dohmen (2012). Investigation of the flow in the impeller side clearances of a centrifugal pump with volute casing. *Journal of Thermal Science* 21(3), 197-208.

Yang, J. H., C. L. Wang and J. P. Li (2003). Mathematical model of flow inside a centrifugal pump casing. *Transactions of the Chinese Society for Agricultural Machinery*, 34(6), 68-72.

Zhang, F. Y. (2013). *Fluid Mechanics*. Beijing, China.

Zhang, S., H. X. Li and D. Xi (2019). Investigation of the Integrated Model of Side Chamber, Wear-Rings Clearance, and Balancing Holes for Centrifugal Pumps. *Journal of Fluids Engineering*, 141(10), 101101.